

The Solar Galactic Environment

Priscilla C. Frisch

University of Chicago, Department of Astronomy and Astrophysics, 5640 South Ellis Avenue, Chicago, IL 60637, USA

Abstract. Combined heliosphere-astronomical data and models enrich our understanding both of effects the solar galactic environment might have on the inner heliosphere, and of interstellar clouds. Present data suggest that $N(\text{Fe}^+)/N(\text{D}^0)$ increases toward the upwind direction of the cluster of interstellar clouds (CLIC) flowing past the Sun. Cloud kinematics and abundances suggest an origin related to a supershell around the Scorpius-Centaurus Association. The solar space trajectory indicates the Sun entered the CLIC gas relatively recently.

1. INTRODUCTION

Combined studies of the heliosphere and surrounding interstellar cloud provide data on the interstellar medium (ISM) both at a single location (scale ~ 500 AU, the heliosphere entry regions) and averaged over sightlines toward nearby stars (scale $\sim 10^6$ AU). Major quests of this relatively young discipline include finding the chemical composition, physical properties, galactography,¹ isotropy, and homogeneity of the CLIC. The ultimate goal is to determine whether historic variations in the boundary conditions of the heliosphere may have affected the inner heliosphere regions and climate of Earth. The astrophysical basis of these questions is addressed in this review.

In our Galactic neighborhood (< 400 pc) interstellar clouds with densities $10^{-5} - 10^5$ cm $^{-3}$, temperatures $10 - 10^6$ K, and velocities $0 - 150$ km s $^{-1}$ are detected. The types and properties of typical clouds include giant molecular clouds ($P=(n(\text{H}^0), n(\text{e}^-), \text{temperature, velocity})=(\sim 5000 \text{ cm}^{-3}, \sim 2 \text{ cm}^{-3}, \sim 20 \text{ K}, \sim 0 \text{ km s}^{-1})$), CO/H₂ clouds ($P=(\sim 500, \sim 0.1, \sim 50, \sim 0)$), cold neutral clouds ($P=(\sim 15, \sim 0.15, \sim 100, \sim 2)$), warm neutral clouds ($P=(\sim 15, \sim 0.20, \sim 3000, \sim 10)$), warm partially ionized clouds such as the LIC ($P=(\sim 0.2, \sim 0.1, \sim 6000, \sim 15-20)$), HII regions ($P=(\sim 0, \sim 10, \sim 10^4, \sim 0)$), intermediate velocity clouds ($P=(\sim 0, \sim 0.3, \sim 8000, \sim 50)$), high velocity clouds ($P=(\sim 0, \sim 0.5, \sim 8000, > 100)$), and tenuous soft-Xray emitting plasma ($P=(\sim 0, \sim 0.0005, \sim 10^6, \text{unknown})$). The intrinsic composition of the ISM is uncertain because of the mass tied up in dust grains ($\sim 1\%$), and abundance variations between cold and warm clouds which persist after correction for ionization [1, 2, 3, 4, 5].

The CLIC appears to be typical warm diffuse low density interstellar material. Warm low density clouds fill $\sim 50\%$ of the galactic disk plane, and hence are the most likely types of clouds to be encountered by the Sun. Also, warm low density clouds are

¹ “Galactography” (the Galactic analog of “geography”) refers to the natural features (e.g. physical properties, morphology) of a region of the Milky Way Galaxy.

generally detected at higher velocities than cold clouds, although this may be partially a line blending effect. Observations of the 21 cm line indicate that $\sim 60\%$ of the H^0 is warm (500–13000 K), and $\sim 50\%$ of the warm material is thermally unstable [6]. This “not strongly absorbing” 21 cm emission is distinctly associated with superbubble shells [7]. The cold gas itself is found in thin sheets with a width-to-thickness aspect ratio of ~ 300 [6]. Hydrogen $\text{H}\alpha$ recombination emission from diffuse warm ionized gas indicates ~ 10 –30% of the ionized gas is associated with low density, warm ($n(\text{H}^0) = 0.2$ – 0.3 cm^{-3} , $T \sim 8000 \text{ K}$) rims of low column density neutral clouds ($< 2 \times 10^{20} \text{ cm}^{-2}$) [8]. If the LIC is a partially ionized cloud rim, the denser cloud may be the neutral material seen upwind toward λ Sco. When low frequency (0.1–10 MHz) radio data are combined with the $\text{H}\alpha$ and pulsar dispersion measurements, a consistent picture emerges indicating the warm ionized gas consists of clumped low density material, $T \sim 7000 \text{ K}$, $< n(\text{e}^-) > \sim 0.23 \text{ cm}^{-3}$, and $\sim 2 \text{ pc}$ radius [9]. The Sun is *required* to be located in such a clump to explain the low frequency turnover in the radio spectrum. UV data also sample the same material, and warm ($\sim 7000 \text{ K}$) low density plasma ($n(\text{e}^-) \sim 0.3 \text{ cm}^{-3}$) is seen at low velocity toward μ Col and at high velocity toward 23 Ori [10, 2]. These generic properties for warm low density gas, the global association between 21 cm emitting warm H^0 gas and superbubble shells, and the CLIC dynamics and abundances (§3), suggest a superbubble origin for the local ISM.

2. THE NEAREST ISM

Radiative transfer models of interstellar gas within $\sim 2 \text{ pc}$ of the Sun, constrained by ISM inside the heliosphere and toward nearby stars, indicate that the LIC at the solar location (SoL) has $n(\text{He}^0) \sim 0.015 \text{ cm}^{-3}$, $n(\text{H}^0) \sim 0.22 \text{ cm}^{-3}$, $n(\text{e}^-) \sim 0.1 \text{ cm}^{-3}$, and $\sim 70\%$ solar abundances [4, 5] (also see the paper by Slavin in this volume). Although these models yield LIC properties that are now better constrained than for any other interstellar cloud, many uncertainties remain. Low column density clouds such as the LIC are highly inhomogeneous because photons efficient for ionizing H^0 ($\sim 13.6 \text{ eV}$) are attenuated sharply in the outer cloud layers. For instance $n(\text{H}^0)/n(\text{He}^0)$ varies by $\sim 50\%$ in the LIC, since H^0 and He^0 are attenuated to $1/e$ at $\log N(\text{H}^0) \sim 17.2$ and 17.7 cm^{-2} respectively (Fig. 1). Partially ionized elements (H, He, Ar, Ne, O, N) and the ratios Mg^+/Mg^0 and C^+/C^{+*} ² provide the most stringent constraints on $n(\text{e}^-)$. Observations of nearby stars give sightline integrated results while ISM data inside of the solar system (He^0 , H^0 , pickup ions and anomalous cosmic rays) anchor the radiative transfer models with data at the SoL. Ionizations predicted at the SoL are $\sim 29\%$ for H, $\sim 27\%$ for O, $\sim 48\%$ for He, $\sim 41\%$ for N, $\sim 88\%$ for Ne, and $\sim 80\%$ for Ar. The best RT models reproduce CLIC data toward ε CMa and yield filtration factors (the fraction of interstellar neutrals successfully penetrating the heliosheath regions) for O, N, Ar, He, and Ar that are consistent with theoretical models [11].

The RT models investigated by Slavin and Frisch ([4, 5], SF02) allow a range of H

² The ratios Mg^+/Mg^0 and C^+/C^{+*} are sensitive to photoionization and collisional processes, respectively.

and He ionization levels and yield $N(\text{H}^0)/N(\text{He}^0)=9\text{--}14$ for LIC-like clouds; this range is consistent with white dwarf data giving $N(\text{H}^0)/N(\text{He}^0)=12\text{--}16$ [12]. The key parameter is the radiation field, shown at cloud surface for Model 2 (SF02, Fig. 1). The observed radiation field consists of contributions from the diffuse soft X-ray background, massive stars such as ϵ CMa, and white dwarf stars. The radiation field must be dereddened to infer the radiation field throughout the LIC from observations at the SoL. Radiation with $\lambda \sim 500$ Å which ionizes He^0 and Ne^0 is the least well constrained observationally. A conductive interface on the cloud surface will contribute emission in this interval (see the Slavin paper). The principal deficiency of the best RT models (chosen to match the widest range of observational data) is the predicted temperature (which is ~ 2000 K too high). However since the temperature is extremely sensitive to the abundance of the primary coolant C^+ , which has abundance uncertainties of $\sim 100\%$ [13], this shortcoming may not be significant.

The interstellar magnetic field at the SoL is poorly understood, and the picture is essentially unchanged since my 1990 talk at the Warsaw COSPAR Symposium [14]. Data on the polarization of nearby stars show a patch of magnetically aligned dust grains in the upstream direction [15], but these results have not been reproduced [16]. From these data the magnetic field direction is parallel to the galactic plane and directed toward $l \sim 70^\circ$. This orientation is consistent with Voyager 3 kHz radio emission data which show a preferred direction parallel to the galactic plane [17]. Possibly the 3kHz emission is related to the draping of the magnetic field around the heliosheath since the classical charged interstellar dust grains polarizing the starlight (radii $\sim 0.1\text{--}0.2$ μm) are deflected around the heliosheath [18, 19]. Polarization strengths vary little in the first 10 parsecs, indicating the polarization occurs within 10 pc of the Sun [14]. The region of maximum starlight polarization is slightly below the ecliptic plane ($\beta = 0^\circ \rightarrow -15^\circ$) but also near the upstream direction in the local standard of rest (LSR) [11]. Weak field strengths ($\sim 1.5\text{--}3.0$ μG) are consistent with both polarization data [14] and Faraday rotation caused by ambient low density weakly ionized ISM [20]. Flux freezing arguments do

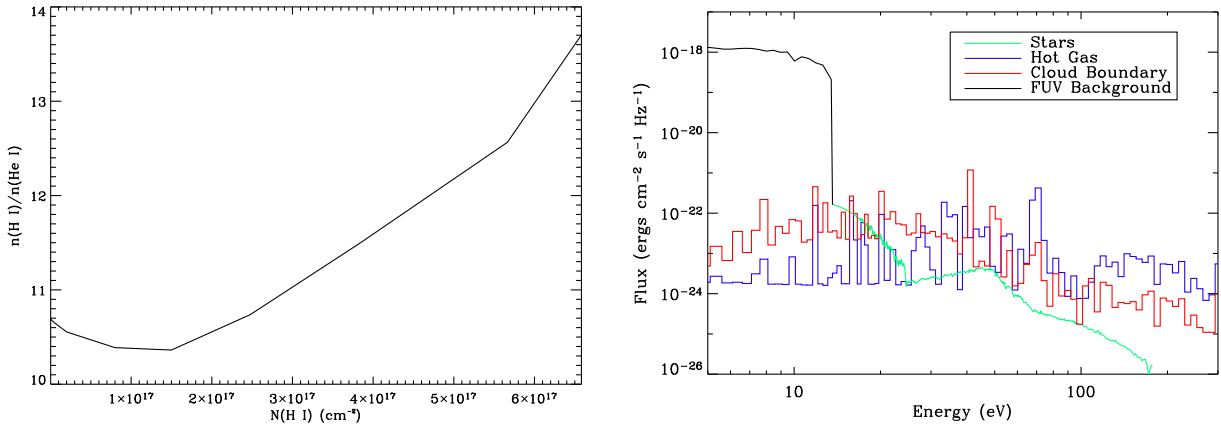


FIGURE 1. **Left:** The ratio between the volume densities of $n(\text{H}^0)$ and $n(\text{He}^0)$ as a function of distance from the LIC surface. The Sun is located at $N(\text{H}^0)=6.5 \times 10^{17} \text{ cm}^{-3}$. **Right:** The interstellar radiation field at the cloud surface after dereddening. Shown are Model 2 results from [4].

not appear valid, since Zeeman splitting studies of the 21 cm H⁰ line show that the parallel component of the magnetic field has little correlation with cloud density [21].

3. THE CLIC

The kinematics and abundance patterns of the CLIC tell us a lot about its origin, in the first case because cloud motions are traced, and in the second because gas-phase abundances are enriched by grain processing in interstellar shocks [22, 23]. Diffuse clouds are identified from the velocity structure of the absorption lines, assuming Doppler broadening from thermal motions plus a catch-all factor interpreted as turbulence. Good data are important for identifying velocity structure since component crowding in velocity space increases exponentially with improvements in instrumental resolution [2]. Observations of UV and optical lines indicate CLIC temperatures are mainly in the range 5000 K to <30000 K, with typical turbulent broadening of $\xi=1.5\text{--}2.5 \text{ km s}^{-1}$. However several local colder clouds ($T<<10^3 \text{ K}$) detected toward stars at distances of $\geq 50 \text{ pc}$ may be part of the Loop I shell [24].

The Sun is embedded in a flow of interstellar cloudlets (the CLIC); it is a robust result that the upstream direction of this flow is toward the Scorpius-Centaurus Association (SCA) [24]. Observations³ of ~ 100 absorption lines sampling the CLIC give a flow velocity with respect to the Sun (heliocentric) of $(l,b,V) = (12.4^\circ, 11.6^\circ, -28.1 \pm 4.6 \text{ km s}^{-1})$. This velocity vector can be converted to the LSR by removing the solar apex motion, giving $(l,b,V) = (331.4^\circ, -4.9^\circ, -19.4 \text{ km s}^{-1})$ and $(l,b,V) = (2.3^\circ, -5.2^\circ, -17.0 \text{ km s}^{-1})$, respectively, for the Standard and cool star apex motions [24].⁴ The large dispersion in the CLIC velocities ($\sim 5 \text{ km s}^{-1}$) indicates a turbulent flow. Regardless of the assumed solar apex motion, the upstream direction is toward the SCA [27, 24], which shows highly structured shell-like H⁰ filaments and a superbubble (Loop I) with radius $>90^\circ$ that dominates the northern sky [28].

The LIC is a cloudlet in the CLIC and it is the only cloudlet with an unambiguous 3D velocity vector because of the Ulysses He⁰ data [29]. The LIC velocity⁵ projects to -17.3 km s^{-1} in the α Cen (1.3 pc) sightline (using Ulysses $n(\text{He}^0)$ data [29]), compared to observed Fe⁺, Mg⁺, D⁰, and Al⁺ velocities ranging between $-17.6 \pm 1.5 \text{ km s}^{-1}$ and $-19.6 \pm 0.6 \text{ km s}^{-1}$ [30, 31, 32]. This small velocity difference has been interpreted to mean the LIC terminates within $\sim 10^4 \text{ AU}$ of the Sun in this direction, but the difference is smaller than the turbulent velocity of $1.5 \pm 0.3 \text{ km s}^{-1}$.

At least five individual clouds are kinematically distinct in this flow, including a cloud at -32 to -35 km s^{-1} (depending on the angular extent of the cloud) and located within 5

³ Only the radial velocity component of the velocity is observed.

⁴ The Standard solar apex motion is 19.7 km s^{-1} toward $l=57^\circ, b=+22^\circ$ [25], while the apex motion determined from Hipparcos observations of cool stars is 13.4 km s^{-1} toward $l=27.7^\circ, b=32.4^\circ$ [26]. The cool-star apex motion reflects the greater age of cool stars which have kinematically relaxed with respect to shorter-lived massive stars.

⁵ The LIC heliocentric upstream vector is $(l,b,V) = (3.3, +15.9, -26.3 \text{ km s}^{-1})$, which converts to an LSR vector $(l,b,V) = (317.8^\circ, -0.5^\circ, -20.7 \text{ km s}^{-1})$ for the Standard, and to $(l,b,V) = (346.0^\circ, +0.1^\circ, -15.7 \text{ km s}^{-1})$ for the cool star apex motion.

pc of the Sun in the solar apex direction [33, 24, 34]. A velocity component denoted the "G-cloud" (for galactic center hemisphere) has been identified to explain a large number of velocity components in the upstream direction, including the cloud toward α Cen (~ 1.3 pc) [35]. The G-cloud, however, appears to result from the overlap in velocity space between distinct cloudlets clustering around the bulk flow velocity of CLIC and at different distances [24]. However if the G-cloud is a single cloudlet, the data shows it must be dense ($n(H^0) > 5 \text{ cm}^{-3}$, [34]).

Inhomogeneities in the ISM were first observed over 50 years ago as systematic increases of $N(\text{Ca}^+)/N(\text{Na}^0)$ with cloud velocity [36]. Similar increases in refractory element (e.g. Fe, Mg, Si, Mn) abundances with cloud velocity are successfully modeled by the shattering and evaporation of interstellar dust grains in shocks [22, 23, 1, 2]. Abundances of Fe^+ and Mg^+ in the CLIC are reproduced by thermal sputtering of dust grains in $\sim 100 \text{ km s}^{-1}$ shocks [18]. However Fe^+ abundances are nonuniform locally, and there is a factor of ~ 6 difference between the maximum value of the ratio Fe^+/D^0 in the upstream direction (toward α Cen A,B and 36 Oph) and minimum value toward the downstream direction (toward $l \sim 160^\circ$ and α Aur, e.g. [30, 32]). Fig. 2 (left) shows $N(\text{Fe}^+)/N(\text{D}^0)$ for absorption components in ~ 30 stars sampling the CLIC plotted against the angle between the star and LSR upstream direction ($l=331^\circ$, $b=-5^\circ$). The Fe^+ abundance increases as the view-direction sweeps upwind, which is consistent with either an ionization or abundance gradient in the CLIC. The alternative possibility is that the Sun is near the boundary of two cloudlets, as Collier et al. [37] have suggested based on data showing two interstellar neutral gas streams at 1 AU. Some components that are exceptions to this trend may sample non-CLIC gas. Components toward HD 333262 and HD 220657 appear to have either anomalously large Fe abundances or ionization. The nearby cloudlets toward λ Sco and α Oph are neutral and significantly denser ($n(H^0) > 2-5 \text{ cm}^{-3}$) than the LIC [38, 34, 39].

Origin and Galactography. The local origin of the weak Ca^+ absorption components observed toward Scorpius and Ophiuchus stars has long been recognized [46, 47, 48], and identified with the interstellar material inside of the solar system [49]. Based on cloud kinematics and refractory abundances, Frisch [27, 45, 50] modeled the local gas as a fragment of superbubble shell around the Scorpius-Centaurus association that has expanded away from SCA region into the low pressure interarm region of the Local Bubble. Combined superbubble shell expansion models and stellar evolution in the SCA subgroups indicates the CLIC properties are consistent with a 4 Myr old superbubble shell⁶ expanding into low density gas remaining from an earlier episode of star formation. Building on the superbubble concept, the CLIC has been modeled as a Rayleigh-Taylor instability formed by the interaction of Loop I and the Local Bubble, which were speculated to have merged 1-10 Myrs ago [51]. These instabilities involve magnetic reconnection in bubble walls which eject ~ 1 pc diameter blobs of gas to the solar vicinity. A third model of the CLIC origin assumes that magnetic flux tubes detach from the walls of the Local Bubble around Sun and spring back toward Sun carrying clumps of gas embedded in relatively strong magnetic fields ($\sim 7 \mu\text{G}$, [52]), but

⁶ In a typographical error, [45] incorrectly lists this age as 400000 years.

predict local magnetic field directions conflicting with the polarization data.

Tracing the solar trajectory backwards in time indicates the Sun has been embedded in the low density interior of the Local Bubble for several million years [54, 55]. The solar trajectory compared to dust clouds in the Local Bubble is shown in Fig. 2 (right), for both the Standard and cool-star apex motions.

I prefer local galactography models which invoke filamentary or sheet-like structures for the CLIC, rather than egg-like models based on smoothing algorithms [56]. The ISM is replete with spectacular filamentary structures, found at all velocities and in both neutral and ionized gas. Emission lines trace relatively young supernova blast waves interacting with low density clouds, such as features seen toward the Cygnus Loop where collisionless shocks accelerate the plasma but not neutral gas [57]. Starlight polarization [15], the EUV source distribution [58], and the high column densities inferred for the G-cloud toward α Oph, λ Sco and HD 149499B [34, 38, 42] all suggest that the CLIC material in the upstream direction is within ~ 10 pc of the Sun.

For the morphology shown in Fig. 3, the Sun emerged from the Local Bubble interior and entered the outflow from the SCA within the past $\sim 10^5$ years, and the LIC within the past 2000–8000 years [59, 50]. Edge effects occurring as the Sun passes through/between cloudlets where magnetic field strength or density may vary appear to perturb the heliosphere and modify the cosmic ray flux in the inner heliosphere, and

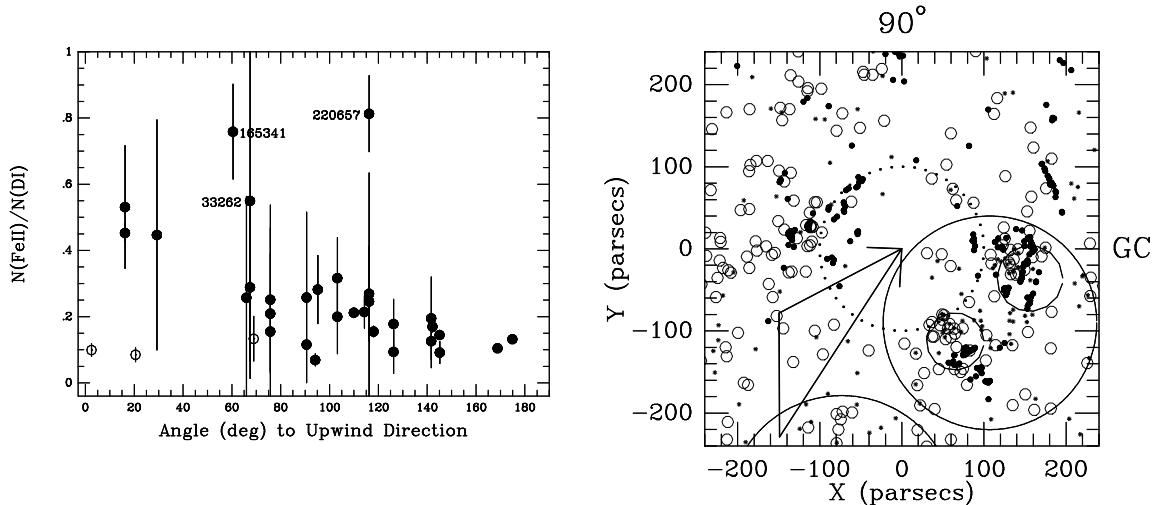


FIGURE 2. **Left:** $N(\text{Fe}^+)/N(\text{D}^0)$ plotted against the angle (in degrees) between the background star and the LSR upwind direction (using the Standard solar apex motion). The plot is based on data from [40, 32, 38, 41, 42]. The G191-B2B component at -9.9 km s^{-1} appears at an angle 174° , and $N(\text{Fe}^+)/N(\text{D}^0)=2.14$, and is not plotted. The open circles represent lower resolution data ($\sim 15\text{--}20 \text{ km s}^{-1}$) toward the stars α Oph, λ Sco and HD 149499B. The remaining data were acquired primarily at resolutions $2\text{--}3 \text{ km s}^{-1}$. For several stars, $N(\text{D}^0)$ is derived from H^0 using $N(\text{D}^0)/N(\text{H}^0)=1.5 \times 10^{-5}$ or $\text{O/H}=400 \text{ ppm}$. **Right:** The space trajectory of the Sun with respect to nearby interstellar clouds within ~ 300 parsecs. Filled dots represent CO and dust clouds from the compilation in [43], open dots represent infrared-bright ($60 \mu\text{m}$) dust surrounding B stars [44], and small dots are nearby early type stars (O–B2). Solar motion is shown for both Standard and cool-star solar apex motions (arrows, see §3), and a dotted circle is drawn at 100 pc. The solid circles are the superbubbles around the Upper Scorpius, Lower Centaurus-Crux and Upper Centaurus Lupus subgroups of the SCA [28, 45]. The past deficit of ISM surrounding the Sun is evident.

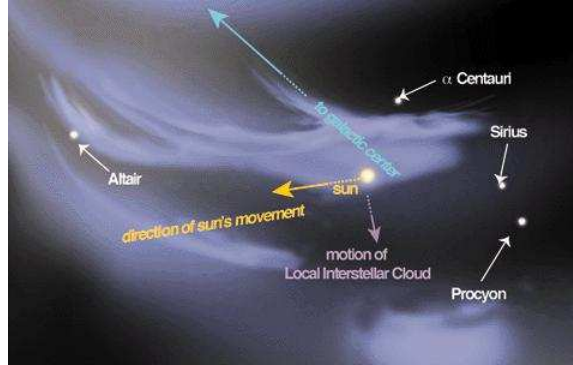


FIGURE 3. The local (<5 pc) ISM filamentary structure shown here is based on the assumption that the LIC velocity vector is parallel to the cloud surface normal [50], which then yields a magnetic field direction nearly parallel to the cloud surface (based on the polarization data [15]). This figure is from [53].

possibly the terrestrial climate [55, 60, 61]. The emergence of *homo sapiens* coincided approximately in time with the Sun's entry into the CLIC, which resulted in a contracted heliosphere and the appearance of anomalous cosmic rays [62, 63]. Cosmic rays at the Earth appear to affect cloud formation [64] and the global electrical circuit [65].

ACKNOWLEDGMENTS

The author would like to thank NASA for research support through the grants NAG5-11005 and NAG5-13107 to the University of Chicago.

REFERENCES

1. Savage, B. D., and Sembach, K. R., *ARA&A*, **34**, 279–330 (1996).
2. Welty, D. E., Hobbs, L. M., Lauroesch, J. T., Morton, D. C., Spitzer, L., and York, D. G., *ApJS*, **124**, 465–501 (2000).
3. Cartledge, S. I. B., Meyer, D. M., Lauroesch, J. T., and Sofia, U. J., *ApJ*, **562**, 394–399 (2001).
4. Slavin, J. D., and Frisch, P. C., *ApJ*, **565**, 364–379 (2002).
5. Frisch, P. C., and Slavin, J. D., *ApJ*, **594**, 844–858 (2003).
6. Heiles, C., and Troland, T. H., *ApJ*, **586**, 1067–1093 (2003).
7. Heiles, C., *ApJ*, **235**, 833–839 (1980).
8. Reynolds, R., Tufte, S., Kung, D., McCullough, P., and Heiles, C., *ApJ*, **448**, 715–726 (1995).
9. Peterson, J. D., and Webber, W. R., *ApJ*, **575**, 217–224 (2002).
10. Howk, J. C., Savage, B. D., and Fabian, D., *ApJ*, **525**, 253–293 (1999).
11. Frisch, P. C., *J. Geophys. Res.*, **108**, 11–16 (2003).
12. Vallerga, J., *Space Sci. Rev.*, **78**, 277–288 (1996).
13. Gry, C., and Jenkins, E. B., *A&A*, **367**, 617–628 (2001).
14. Frisch, P. C., “Characteristics of the local interstellar medium,” in *Physics of the Outer Heliosphere*, pp. 19–22 (1990).
15. Tinbergen, J., *A&A*, **105**, 53–64 (1982).
16. Leroy, J. L., *A&A*, **274**, 203–213 (1993).
17. Kurth, W. S., and Gurnett, D. A., *J. Geophys. Res.*, **108**, 2–16 (2003).

18. Frisch, P. C., Dorschner, J. M., Geiss, J., Greenberg, J. M., Grün, E., Landgraf, M., Hoppe, P., Jones, A. P., Krätschmer, W., Linde, T. J., Morfill, G. E., Reach, W., Slavin, J. D., Svestka, J., Witt, A. N., and Zank, G. P., *ApJ*, **525**, 492–516 (1999).
19. Linde, T. J., and Gombosi, T. I., *J. Geophys. Res.*, **105**, 10411–10418 (2000).
20. Rand, R. J., and Kulkarni, S. R., *ApJ*, **343**, 760–772 (1989).
21. Heiles, C., and Troland, T. H., *ApJ*, **586**, 1067–1093 (2003).
22. Jones, A. P., Tielens, A. G. G. M., Hollenbach, D. J., and McKee, C. F., *ApJ*, **433**, 797–810 (1994).
23. Jones, A. P., Tielens, A., and Hollenbach, D. J., *ApJ*, **469**, 740–764 (1996).
24. Frisch, P. C., Grodnicki, L., and Welty, D. E., *ApJ*, **574**, 834–846 (2002).
25. Allen, C. W., *Astrophysical Quantities*, AthlonePress, 1973.
26. Dehnen, W., and Binney, J. J., *MNRAS*, **298**, 387–394 (1998).
27. Frisch, P. C., *Nature*, **293**, 377–379 (1981).
28. de Geus, E. J., *A&A*, **262**, 258–270 (1992).
29. Witte, M., Banaszkiewicz, M., Rosenbauer, H., and McMullin, D., *Adv. Space Res.*, *in press* (2004).
30. Linsky, J. L., and Wood, B. E., *ApJ*, **463**, 254–270 (1996).
31. Wood, B., Linsky, J., Müller, H., and Zank, G., *ApJ*, **547**, L49–L52 (2001).
32. Redfield, S., and Linsky, J. L., *ApJ*, **602**, 776–802 (2004).
33. Lallement, R., Vidal-Madjar, A., and Ferlet, R., *A&A*, **168**, 225–236 (1986).
34. Frisch, P. C., *ApJ*, **593**, 868–873 (2003).
35. Lallement, R., *Space Sci. Rev.*, **78**, 361–374 (1996).
36. McRae Routly, P., and Spitzer, J. L., *ApJ*, **115**, 227 (1952).
37. Collier, M. R., Moore, T. E., Simpson, D., Roberts, A., Szabo, A., Fuselier, S. A., Wurz, P., Lee, M. A., and Tsurutani, B. T., *Adv. Space Res.*, *in press* (2004).
38. York, D. G., *ApJ*, **264**, 172–195 (1983).
39. Mueller, H. R., Zank, G. P., and Frisch, P. C., *in preparation* (2004).
40. Redfield, S., and Linsky, J. L., *ApJS*, **139**, 439–465 (2002).
41. Frisch, P. C., York, D. G., and Fowler, J. R., *ApJ*, **320**, 842–849 (1987).
42. Lehner, N., Jenkins, E., Gry, C., Moos, H., Chayer, P., and Lacour, S. A&A, **595**, 858–879 (2003).
43. Dutra, C. M., and Bica, E., *A&A*, **383**, 631–635 (2002).
44. Gaustad, J. E., and van Buren, D., *Pub. Astron. Soc. Pacific*, **105**, 1127–1140 (1993).
45. Frisch, P. C., *Space Sci. Rev.*, **72**, 499–592 (1995).
46. Munch, G., and Unsold, A., *ApJ*, **135**, 711–715 (1962).
47. Herbig, G. H., *Zeitschrift Astrophysics*, **68**, 243–277 (1968).
48. Marschall, L. A., and Hobbs, L. M., *ApJ*, **173**, 43–62 (1972).
49. Adams, T. F., and Frisch, P. C., *ApJ*, **212**, 300–308 (1977).
50. Frisch, P. C., *Space Sci. Rev.*, **78**, 213–222 (1996).
51. Breitschwerdt, D., Freyberg, M. J., and Egger, R., *A&A*, **361**, 303–320 (2000).
52. Cox, D. P., and Helenius, L., *ApJ*, **583**, 205–228 (2003).
53. Frisch, P. C., *American Scientist*, **88**, 52–59 (2000).
54. Frisch, P., and York, D. G., “Interstellar clouds near the Sun,” in *The Galaxy and the Solar System*, U. Arizona Press, pp. 83–100 (1986).
55. Frisch, P. C., <http://xxx.lanl.gov/pdf/astro-ph/9705231> (1997).
56. Linsky, J. L., Redfield, S., Wood, B. E., and Piskunov, N., *ApJ*, **528**, 756–766 (2000).
57. Patnaude, D. J., Fesen, R. A., Raymond, J. C., Levenson, N. A., Graham, J. R., and Wallace, D. J., *AJ*, **124**, 2118–2134 (2002).
58. Warwick, R. S., Barber, C. R., Hodgkin, S. T., and Pye, J. P., *MNRAS*, **262**, 289–300 (1993).
59. Frisch, P. C., *Science*, **265**, 1423–1427 (1994).
60. Frisch, P., Mueller, H., Zank, G., and Lopate, C., *Galactic Environment of Sun and Stars: Interstellar and Interplanetary Material*, Cambridge: Cambridge University Press, *in press* (2004).
61. Florinski, V., Zank, G. P., and Axford, W. I., *Geophys. Res. Lett.*, **30**, 5–1 (2003).
62. Frisch, P., *Galactic Environments of Sun and Cool Stars*, Editions Frontieres, pp. 3–10 (1999).
63. Mueller, H. R., Zank, G. P., and Frisch, P. C., “Effect of Different Possible Interstellar Environments on the Heliosphere: A Numerical Study,” in *The Outer Heliosphere: The Next Frontiers*, edited by K. Scherer, COSPAR Colloquia Series, 11., p. 329 (2001).
64. Carslaw, K. S., Harrison, R. G., and Kirkby, J., *Science*, **298**, 1732–1737 (2002).
65. Roble, R. G., *J. Atmosph. Terres. Phys.*, **53**, 831–847 (1991).